



ELSEVIER

Contents lists available at ScienceDirect

Electrochimica Acta

journal homepage: www.elsevier.com/locate/electacta

Research Paper

Influence of electrochemical cycling on the rheo-impedance of anolytes for Li-based Semi Solid Flow Batteries



A. Narayanan^{a,*}, D. Wijnperlé^a, F. Mugele^a, D. Buchholz^{b,c}, C. Vaalma^{b,c}, X. Dou^{b,c}, S. Passerini^{b,c}, M.H.G. Duits^a

^a Physics of Complex Fluids group, University of Twente and MESA+ Institute, PO Box 217, 7500 AE Enschede, The Netherlands

^b Helmholtz-Institute Ulm, Helmholtzstraße, 11, 89081 Ulm, Germany

^c Karlsruhe Institute of Technology (KIT), P.O. Box 3640, 76021 Karlsruhe, Germany

ARTICLE INFO

Article history:

Received 15 May 2017

Received in revised form 3 August 2017

Accepted 5 August 2017

Available online 12 August 2017

Keywords:

Semi Solid Flow Battery

Solid Electrolyte Interface

Carbon Black

Rheology

Impedance Spectroscopy

ABSTRACT

The recently launched concept of Semi-Solid Flow Batteries (SSFBS) shows a strong potential for flexible energy storage, but the liquid-dispersed state of the electrode materials introduces several aspects of which a scientific understanding is lacking. We studied the effect of electrochemical cycling on the rheological and electrical properties of a SSFB anolyte containing $\text{Li}_4\text{Ti}_5\text{O}_{12}$ (LTO) and Ketjen Black (KB) particles in EC:DMC solvent with 1M LiPF_6 , using an adapted rheometer that allows in situ electrochemical cycling and electrical impedance spectroscopy. Charging (lithiation) caused a reduction in the electronic conductivity, yield stress and high shear viscosity of the fluid electrode. For mildly reducing voltages (1.4 V), these changes were partially reversed on discharging. For more reducing voltages these changes were stronger and persistent. The finding of comparable trends for a fluid electrode without the LTO, lends support to a simplistic interpretation, in which all trends are ascribed to the formation of a surface layer around the conductive KB nanoparticles. This Solid Electrolyte Interphase (SEI) insulates particles and reduces the van der Waals attractions between them. SEI layers formed at less reducing voltages, partially dissolve during the subsequent discharge. Those formed at more reducing voltages, are thicker and permanent. As these layers increase the electronic resistance of the fluid electrode by (more than) an order of magnitude, our findings highlight significant challenges due to SEI formation that still need to be overcome to realize SSFBs.

© 2017 The Authors. Published by Elsevier Ltd. This is an open access article under the CC BY license (<http://creativecommons.org/licenses/by/4.0/>).

1. Introduction

Semi-Solid Flow Batteries (SSFBS), as recently introduced by Duduta et al. [1], comprise a promising addition to the spectrum of rechargeable battery systems. The advantages of SSFBs over conventional batteries lie in the decoupling of power (cell size) and energy (tank size), and the potential for adjusting the chemistry of the system during operation. In particular non-aqueous SSFB systems are interesting, since they offer much higher energy densities as compared to more conventional aqueous redox flow systems [1]. The ability of non-aqueous SSFBs to provide and store energy in a flexible way makes them particularly promising for grid applications.

However, a key aspect in which SSFBs are yet unproven is their performance after repeated electrochemical cycling. While many SSFBs use the same materials [1,2] as conventional lithium-ion batteries, they may potentially degrade in different ways due to the dispersed state of the solid matter. In SSFBs (de)lithiation takes place in electrochemically active particles while the electrons are transported to the current collectors via conductive nanoparticles (CNPs). The occurrence of both particles in the (sub)micron size range has several consequences: i) the surface-to-volume ratio is relatively large, and ii) Brownian motion and interparticle interactions now play a role. Electrochemistry induced changes can therefore manifest themselves in different ways. They can directly affect individual particles (e.g. electronic conductivity, lithium uptake) but also collective effects are possible, because colloidal particles show a tendency for self-assembly into a microstructure. The colloidal interactions, which drive this assembly, are likely to be affected by the electrochemical cycling, and since the structure is kept dynamic by Brownian motion

* Corresponding author.

E-mail address: a.narayanan@utwente.nl (A. Narayanan).

and/or shear flow, the microstructure may adapt to electrochemical changes.

While the precise microstructure of SSFB fluids is still to be ascertained, the generally accepted view [1–3] is that in the absence of flow, the CNPs assemble into a branched percolating network. This network provides electronic conduction and sustains static forces, thereby resisting the sedimentation of particles. In flow, the network gets broken down into agglomerates with a size that depends on the shear rate [3–5]. The contribution of active particles to the microstructure is less understood. They are expected to behave like a disordered fluid that surrounds the CNP network. This lack of order is inferred from the insignificance of both attractive and long-ranged repulsive forces; the former since otherwise the viscosity would be very high, the latter from the strong screening by the dissolved salt [6].

These differences between SSFBs and conventional lithium-ion batteries raise the question, how degradation processes such as volume and structural changes of the active materials upon (de-) lithiation [7] or the formation of solid electrolyte interface (SEI) [8,9] affect SSFBs. Several consequences of such processes for fluid electrodes are conceivable. Considering the CNP network, both the nature of the interparticle contacts and their number density can change: the former as a consequence of surface processes, and the latter due to (for flow batteries inherent) mechanical rejuvenation: shear-induced fragmentation of the CNP network creates a possibility for the fragments to re-assemble into a different microstructure when the fluid returns to the quiescent state³. Macroscopically, the electronic conductivity and the yield stress are likely affected by these microscopic processes. While critically relevant to SSFBs, the above phenomena can potentially also affect other types of battery systems that use self-assembling colloidal particles, such as polysulphide [10] and carbon free [11] flow batteries. Recent work on carbon slurry based iron redox flow batteries has shown electronic conductivity enhancement through changes in the interparticle contacts due to iron plating [12].

The objective of the present work is twofold: to quantify changes in rheological and electrical performance due to repeated electrochemical cycling, and to gain a mechanistic understanding of these macroscopic changes. To achieve these goals, a commercial rheometer was extended to allow parallel electrical impedance measurements, as well as a controlled cycling of the fluid electrodes via the inclusion of a lithium counter electrode. The studied fluid electrode consists of a mixture of Ketjen Black (KB) and $\text{Li}_4\text{Ti}_5\text{O}_{12}$ (LTO) particles dispersed in EC:DMC 1:1 with 1 M LiPF_6 . LTO has previously been identified as a promising active material for SSFBs [13] as lithiation occurs at about ~ 1.55 V vs Li/Li^+ , within the safe operating range of the non-aqueous electrolyte [2,14,15]. To examine the role of electrochemical state (and history), we cycle the fluid electrode to a series of increasingly reducing voltages, measuring the rheological and electrical properties before and after each charge and discharge step. Comparisons are also made before and after mechanical rejuvenation, to probe the changes in self-assembly. To facilitate interpretation of the various changes we also make a comparison between the results for the KB-LTO electrode, and a fluid electrode without the LTO.

2. Materials and Methods

2.1. Fluid Electrode Preparation

Ethylene carbonate (EC) and dimethyl carbonate (DMC) were obtained from Sigma Aldrich (anhydrous, 99%+ purity). Binary mixtures of EC and DMC were 1:1 by mass. LP30 (EC:DMC 1:1 with 1 M LiPF_6) was obtained from BASF. Ketjen Black EC 600JD powder (KB) was obtained from AkzoNobel. $\text{Li}_4\text{Ti}_5\text{O}_{12}$ powder was obtained

from Südcemie. Lithium foil was purchased from Alfa Aesar (99.9%). All sample preparations and experiments were carried out in an MBraun Argon-filled glove box (O_2 , H_2O below 1 ppm). Two fluid electrodes were prepared: a mixture of 1 wt.% KB and 5 wt.% LTO, and a reference sample at 1 wt.% KB. The dry particles were first wetted by EC-DMC solvent for 8 hours to improve their dispersibility; from an earlier study it is known that KB is colloidally unstable in carbonate solvent with large amounts of salt [6]. The KB reference contained 2.9 wt.% KB while for the mixture it was 2.6 wt.% KB and 13.4 wt.% LTO at this stage. Afterwards, LiPF_6 salt (Alfa Aesar (98%)) was added via a concentrated solution ($\text{LP30} + \text{LiPF}_6$) to reach a concentration of 1 M (viscosity 4 mPas [16]). After an additional 8 h, the samples were homogenized by rotor stator mixing (Ultraturrax) at 15000 rpm for 2 min, and loaded in the rheo-impedance setup.

2.2. Cycling-rheo-impedance setup

Electrochemical cycling and rheo-impedance measurements were performed on a stress controlled rheo-meter (Haake RS 600) with a home-built adaptation (Fig. 1) comprising an extension of a previously described system [3]. Briefly, the 60 mm parallel plate geometry of the rheometer was used as a base. A copper plate attached to the upper rheometer rotor served as a shearing surface, current collector and electrode for electrical impedance spectroscopy (EIS). A perforated stainless steel (316) plate was used as the bottom shearing surface. Due to the small size (1 mm radius) and fraction (< 40%) of the holes, rheological measurements could be performed with reasonable accuracy (within 5%; test with 1.231 Pas and 0.01 Pas calibration oils). This plate also served as a second electrode for EIS. A Celgard 2500 separator was used to separate the perforated plate from a second compartment with a lithium foil (on a titanium current collector). This allowed the foil to be in contact the electrolyte but not the particles. In the solvent trap of the rheometer (not shown), mercury was used as a working fluid to ensure a low friction and low noise electrical connection to the rotating upper geometry [3]. During rheological tests all electrodes were disconnected.

EIS measurements were performed (between the upper and perforated plate, with S1 closed and S2 open) in a four-terminal configuration. The perforated plate was excited by a sinusoidal voltage of < 50 mV in the frequency range from 10 MHz to 0.01 Hz. Amplitude sweeps on the KB-only fluid had indicated that the response was linear (and hence the impedances the same) at least up to 100 mV (Note: these voltages were applied at the HF2 output. The actual voltage across the sample was typically much smaller). Currents were measured by a transimpedance amplifier (HF2CA, Zurich Instruments) on the virtually grounded rotor. A buffer pre-amplifier (HF2TA, Zurich Instruments) was used to measure the potential difference between the perforated plate and the rotor. An impedance spectroscopy (HF2IS, Zurich instruments) was used to

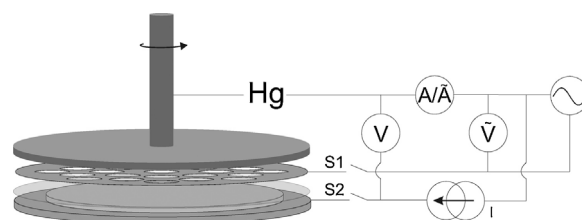


Fig. 1. Schematic of rheo-impedance setup. dark grey: upper geometry, perforated plate, bottom current collector translucent gray: membrane, beige: lithium foil on current collector. Either switch S1 or S2 is closed, to allow EIS or electrochemical cycling.

extract the complex impedance from the current and voltage signals. The lithium electrode was allowed to float (it was disconnected from the external circuit) during these measurements. Frequency dependent parasitic impedances of the setup were calibrated out using the “open short” technique [17,18].

Samples were electrochemically cycled (with S2 closed) using the lithium foil ($> 30 \text{ cm}^2$) as a counter electrode and the Celgard membrane as an ion permeable medium. As the maximum current was low ($< 50 \mu\text{A cm}^{-2}$) the total polarization was below 50 mV [19,20]. Currents were measured through a 50Ω resistor. The potential of the perforated plate was allowed to float during cycling. Galvanostatic and potentiostatic charging were performed using the impedance spectroscope. Custom LabVIEW codes were used to perform cycling and EIS and to synchronize them with rheological measurements.

2.3. Experimental Protocol

All surfaces in contact with the sample (excluding the lithium foil and the separator) were sand papered and thoroughly cleaned outside the glovebox prior to the experiment. They were subsequently wetted with DMC for 15 min prior to sample loading in the glovebox. Cycling-rheo-impedance experiments were performed with a gap of $250 \mu\text{m}$ between upper current collector and perforated plate. To avoid sample variations due to differences in shear history [3], we pre-sheared each sample at 1000 s^{-1} for 200 s, and subsequently allowed them 200 s of rest. This ‘mechanical rejuvenation’ was applied before each cycling (charging or discharging) step. Rheo-impedance measurements were carried out both before and after this treatment. The lithium electrode was disconnected during rheo-impedance measurements. A scheme of the protocol is given in Fig. 2.

To indicate the electrochemical history, we code our samples as follows: (Voltage window number). (Cycle number). (Charge (lithiation)/Discharge (delithiation) step). The pristine state is denoted as P. For example, code 2.3.C represents the state reached in the 2nd voltage window after charging the fluid for the 3rd time under these conditions. Moreover, each sample has two mechanical states: before or after mechanical rejuvenation.

Samples were (dis-) charged galvanostatically using a current of 1.5 mA. Assuming an LTO concentration of (5 wt.% =) 0.121 g ml^{-1} and a specific capacity of 175 mAh g^{-1} , this corresponds to a rate of about C/10. Once the cutoff voltage was reached, the voltage was held until the current fell below 0.5 mA. Thereafter EIS measurements were performed, taking into account the aforementioned mechanical protocol. Next the yield stress was measured by ramping up the shear stress (62 s per stress decade) while measuring the strain. The $\log(\text{strain})$ versus $\log(\text{stress})$ curve was fitted with two straight lines and the stress at the intersection was taken to be the yield stress [21]. The flow curve was subsequently measured by pre-shearing at 1000 s^{-1} for 200 s and

then slowly stepping the shear rate downwards from 1000 s^{-1} (at 20 steps per shear rate decade). After an equilibration time of 20 s the viscosity was averaged over one second. Six charge and discharge half-cycles were performed for each voltage window. At the end of the experiment, samples were recovered, dried at 60°C and then analyzed *post mortem* outside the glovebox.

3. Results and Discussion

SSFB fluid electrodes conduct through ionic and electronic pathways [1,4]. As the metal current collectors that enclose the fluid electrode are ionically blocking but electronically reversible, these two contributions can (in principle) be separated using impedance spectroscopy [3,22]. The electronic resistance of the fluid electrode's percolated particle network (with some contributions from the current collector interface [3,4]) corresponds to the low-frequency limit of the real impedance. Experimental timescales do not always allow access to this limit, and therefore the low frequency real impedance (LFRI see Fig. 3 panel B) at 0.01 Hz was taken as practical measure (suitable for identifying trends) of the electronic resistance. Further justification of this approach will be presented in Fig. 4B, where we also fit LFRI values using an equivalent electrical circuit model.

Fig. 3 shows the impedance, yield stress and viscosity (from now on termed together as rheo-impedance) of a fluid electrode containing 1 wt.% KB and 5 wt.% LTO, cycled between 1.4–2.5 V and 1.0–2.5 V. Most measurements (solid symbols) were performed after mechanical rejuvenation of the fluid; we will focus on these first.

In regime I, with a less reducing cut-off of 1.4 V, both the LFRI and the yield stress show an alternating behavior on cycling, with a higher LFRI and a lower yield stress at 1.4 V as compared to 2.5 V. The difference in the LFRI at the two states of charge becomes progressively smaller upon cycling, while the difference in yield stress remains roughly the same. Subsequent cycling in regime II, with a cutoff of 1.0 V, leads to strong changes. The LFRI triples, and further alternation is suppressed. The yield stress roughly halves, but here the alternations remain (Fig. 3C). The loss of alternations in the measured LFRI may be due to experimental limitations: as shown by the Nyquist plot (Fig. 3B), the time constant of the low frequency arc shows a large increase, thereby compromising the sensitivity of the LFRI to the electronic resistance.

Changes in the rheological properties are reflected in not just the yield stress but also the flow curves. Inspection of the latter reveals that the shear-rate dependence of the viscosity is rather similar for all samples (inset Fig. 3D). This allows representation of the effects of electrochemical cycling via a viscosity scale-factor VSF (main panel of Fig. 3D). The yield stress and VSF show a similar dependence on the electrochemical state; lithiation lowers both quantities and vice versa for delithiation. Changing to regime II, i.e. the cycling between 2.5 V–1.0 V, the yield stress and viscosity reduce. Again these changes correlate well with the higher LFRI, with the exception that alternations remain in the yield stress and VSF. This may be due to the aforementioned issue with the LFRI.

Interpretation of the progressive changes in rheo-impedance of the fluid after cycling is not trivial. One aspect hereof is that the duration of the charge and discharge was not the same for each cycle (see SI Fig. S1, and Table TS1). For this reason, only relative changes caused by electrochemical cycling (and mechanical rejuvenation) will be discussed. Furthermore, the measurements are performed in a complex system, consisting of several instrumental parts and a multicomponent fluid electrode. Analyzing the electrical and rheological data in conjunction, the scope of interpretation can however be narrowed down. Importantly, the electrical and mechanical signals originate from the same system,

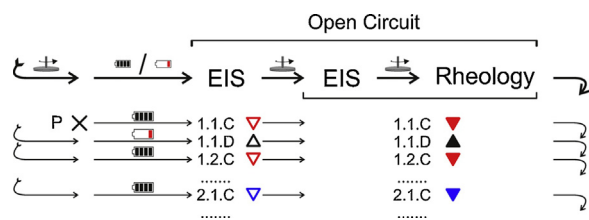


Fig. 2. Schematic of the (repetitive) measurement protocol. Pictograms indicate mechanical rejuvenation and electro-chemical (dis)charging. The rejuvenation serves to create a reference state by breaking down the particle agglomerates and letting them re-assemble again. Since EIS does not involve mechanical deformation, measurements before and after rejuvenation can be compared.

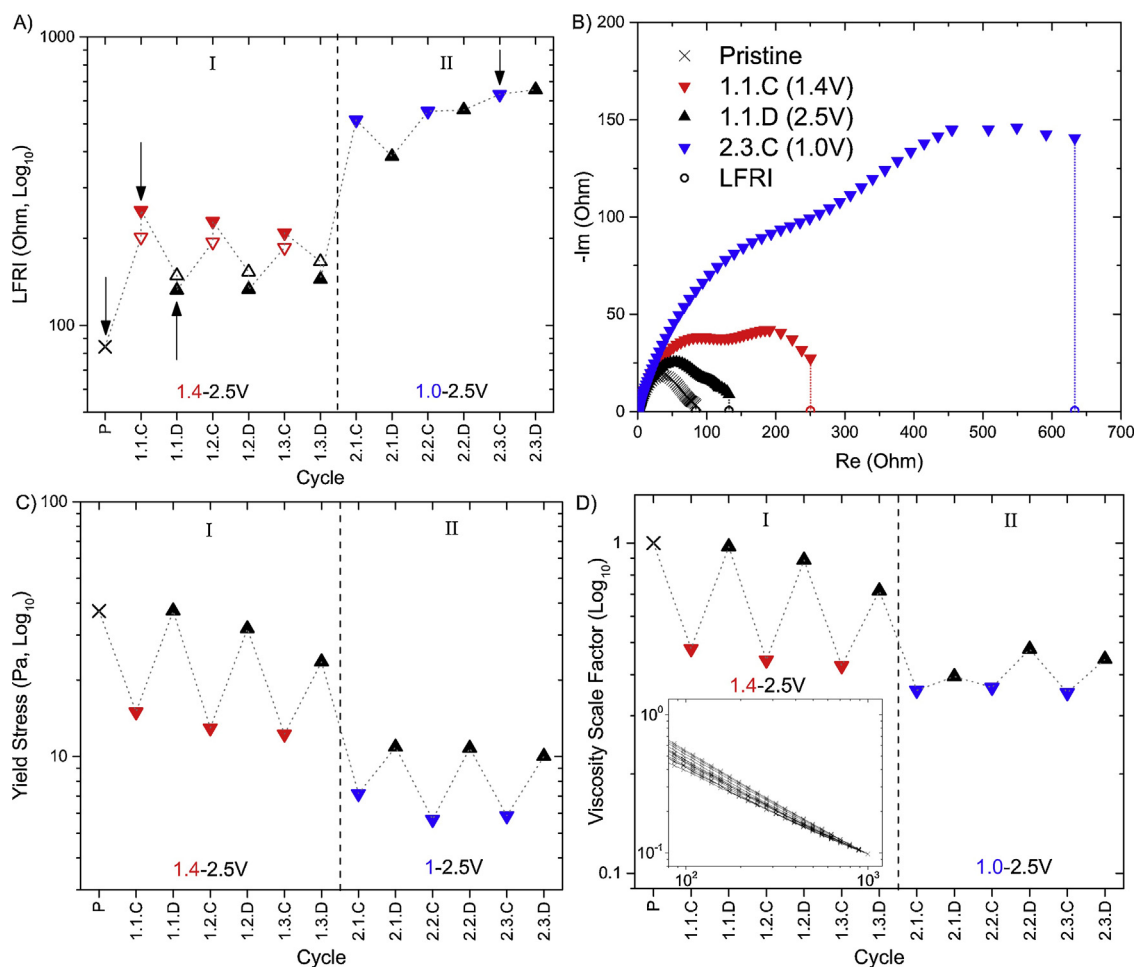


Fig. 3. Rheo-impedance of 1 wt.% KB + 5 wt.% LTO fluid electrode subject to cycling in different voltage ranges. (X): pristine state, (Δ): discharged to 2.5V, (∇): charged to indicated voltage. Open symbols: not mechanically rejuvenated, Closed symbols: mechanically rejuvenated. A) Low frequency real impedance from EIS spectra obtained at the end of charge or discharge. B) Nyquist plots of data points marked with arrows in A. The dotted lines connect the lowest frequency impedance to the LFRI C) Yield stress. D) Viscosity scale factor: the factor with which the viscosity at 1000 s^{-1} has to be multiplied to coincide with that of the pristine state. The inset shows the flow curves (viscosity in Pa s vs. shear rate in s^{-1}) after multiplication with the VSFs.

comprising a bulk fluid between the same two metal plates (the upper current collector and the perforated plate).

This still leaves the question, whether contributions from the metal-fluid interfaces can be neglected or not. A significant interfacial contribution to the rheological signal would require a mechanically weak layer near the rheometer geometry walls (e.g. due to depletion of particles or weak particle-wall interactions). There are however no indications for this. First, the yield stress curves (see SI Fig. S3) indicate an initial elastic deformation and finite strain at yield (also for samples with a very high LFRI). This corresponds well to a gap-spanning network, whereas a weak interfacial layer would already yield (i.e. flow) at an infinitesimal strain. Secondly, the viscosities (at high shear rates) change appreciably with each cycling step, implying that the forces responsible for particle agglomeration should do the same³. This is only possible if the particles themselves undergo changes. The absence of a particle-depleted layer at the metal plates, as inferred from the rheology, suggests that the LFRI signal is dominated by the fluid bulk. From a different perspective, since the gap ($250\text{ }\mu\text{m}$) between the measuring surfaces for EIS spans $O(1000)$ particle diameters, the number of particle contacts involved in an electron conduction path has to be very large, as compared to the single particle-metal contact per current collector. It is thus appropriate to seek an explanation of the observations in Fig. 3 in terms of changes to the particles (and not the enclosing metal surfaces).

Since SSFB electrodes are multi-component mixtures, the effects of electrochemical cycling are not limited to just one component. However, additional observations help identify the most dominant changes. Examination of the LTO particles (both in pristine state, and after cycling) revealed that no structural decomposition could be detected with XRD (see SI Fig. S4). The higher electronic conductivity of carbon blacks compared to LTO suggests that they will have a dominant influence on the suspension electronic conductivity. Moreover, the different rheologies of suspensions of only KB (yield stress, higher viscosity) and only LTO (no yield stress, lower viscosity) in the same solvent (see SI Fig. S5) suggests that the carbon black particles have a dominant influence on the rheology. In absence of an all-encompassing model for how electronic conductivity and yield stress are generated in the fluid electrodes, it is thus very reasonable to assume that the dominant contribution to both signals comes from the KB.

To demonstrate this further, we consider a similar measurement on a sample that contains only KB as a particulate component (Fig. 4). This sample was cycled in four voltage ranges, where the first two correspond to those of the KB-LTO fluid electrode (see SI Fig. S2 and Table TS 1). In regime I (1.4V cutoff), the behavior of the KB fluid electrode is similar to that of the KB-LTO fluid electrode. In the subsequent, more reducing regimes II and III (with cutoff voltages of 1.0 and 0.8V respectively), the differences between the

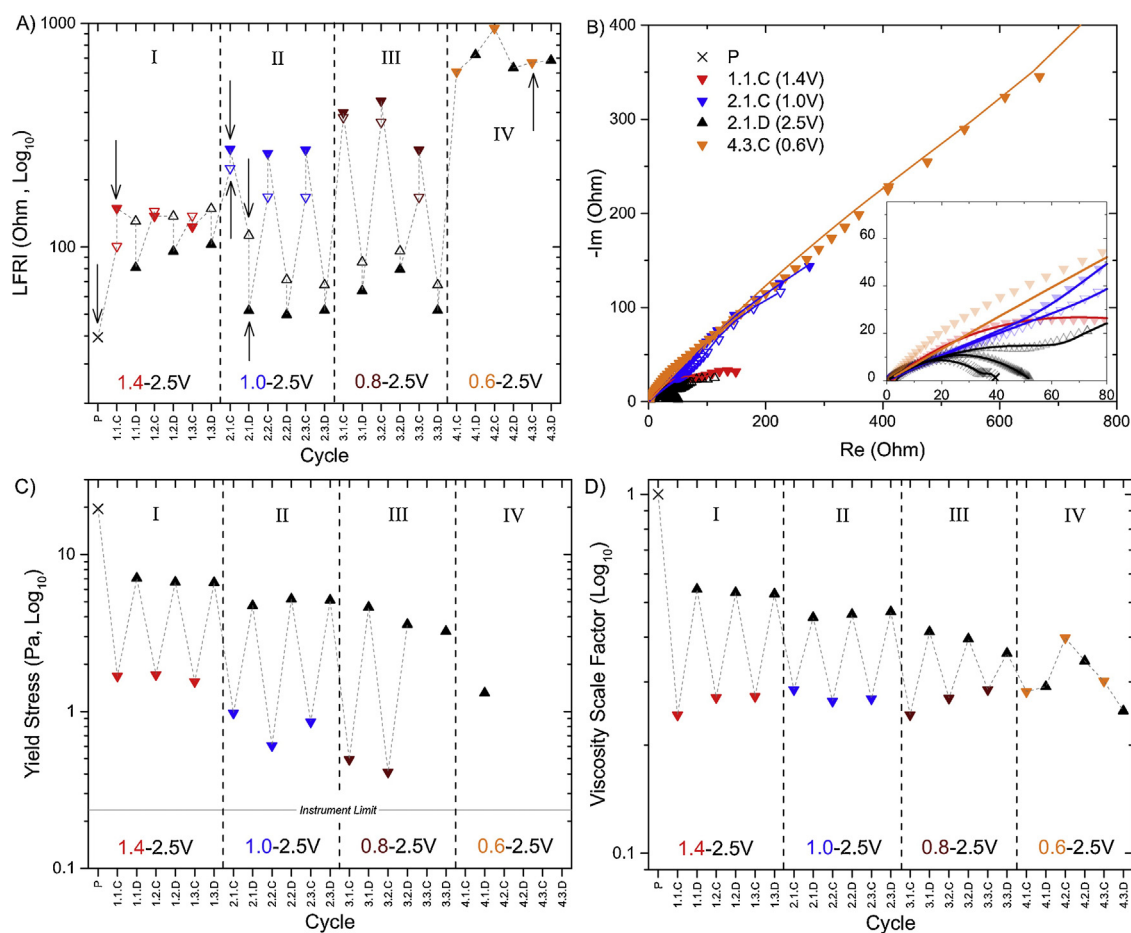


Fig. 4. Rheo-impedance of 1 wt% KB fluid electrode subject to cycling. Symbols are the same as Fig. 3. A) LFRl. B) Nyquist plots of data points marked with arrows in A and fits (described later) using the equivalent circuit in Fig. 7 C) Yield stress. D) Viscosity scale factor, defined similarly as in Fig. 3.

‘charged’ (reduced) and ‘discharged’ states progressively become larger, spanning almost an order of magnitude for both the LFRl and yield stress. The alternation of both properties appears to be repeatable in regimes II and III. However, cycling in regime IV with a cutoff of 0.6V (well outside the stability window of the electrolyte) results in a massive increase in the LFRl and decrease in the yield stress and VSF. No clear trends are observed in the LFRl or rheological properties for subsequent cycles.

While the voltage ranges appear slightly shifted, the behavior of the KB-only fluid electrode qualitatively agrees with that of the KB-LTO mixture. We can thus attribute the behavior of both systems to the KB network. Within this focused interpretation, the LFRl trends in Figs. 3 and 4 can be rationalized by the formation of an insulating SEI layer around the KB particles upon exposure to reducing voltages, and a partial dissolution of this layer during delithiation (2.5V). Recent studies have demonstrated that the composition and properties of the SEI depend on the potential versus lithium where it is formed [23–25]. At higher voltages, a sparse and less insulating SEI layer composed of organic compounds (more prone to dissolution) is formed. At lower potentials; a thicker, denser, less soluble, and more insulating layer composed of inorganic compounds gets formed.

Our interpretation that a layer gets formed on the carbon during charging and it partially dissolves during subsequent discharging, is further corroborated by an experiment using ellipsometry. Here a copper substrate coated with a sputtered carbon layer was immersed in EC:DMC 1:1 + 1 M LiPF₆, and exposed to voltages of

1.0 and 2.5V with respect to an immersed lithium foil. Ellipsometric angles ψ and Δ were measured in-situ with a Woollam M2000 ellipsometer, as a function of wavelength. Fig. 5 shows the evolution of Psi ψ and Delta Δ (for a typical wavelength of 800 nm) as a function of electrochemical history. The pristine sample (in the absence of current) shows fairly constant ψ and Δ values that are in agreement with a 81 nm thick carbon layer on bulk copper. Strong and ongoing changes in both ellipsometric angles are observed when the voltage is set to a 1.0V (‘charging’) while setting the voltage to 2.5V (‘discharging’) results in a partial recovery of both Psi and Delta angles. Since Cu and carbon do not dissolve under these conditions, the changes in ψ and Δ during exposure to 1.0V must be due to the deposition of a new material on the substrate. This makes it likely that the partial reversal of these changes on exposure to 2.5V are due to a partial dissolution of this layer. A detailed quantitative analysis of the (ψ, Δ) data by comparison to optical models for the layer structure is possible, but the choice of an appropriate model in conjunction with the limited additional information about the layer’s optical properties present challenges. A simplistic model which can describe our wavelength dependent (ψ, Δ) data is a 5-layer stack: (bulk) Cu-C-an intermediate layer-SEI-(bulk) electrolyte. The intermediate layer represents a linear transition in optical properties from that of carbon to that of the SEI, accounting for intermixing. Using optical parameters for the SEI as given in McArthur et al. [26], the model produces the thicknesses in Fig. 5 (inset). It can be seen that SEI starts to form when the voltage is switched to 1.0V and when

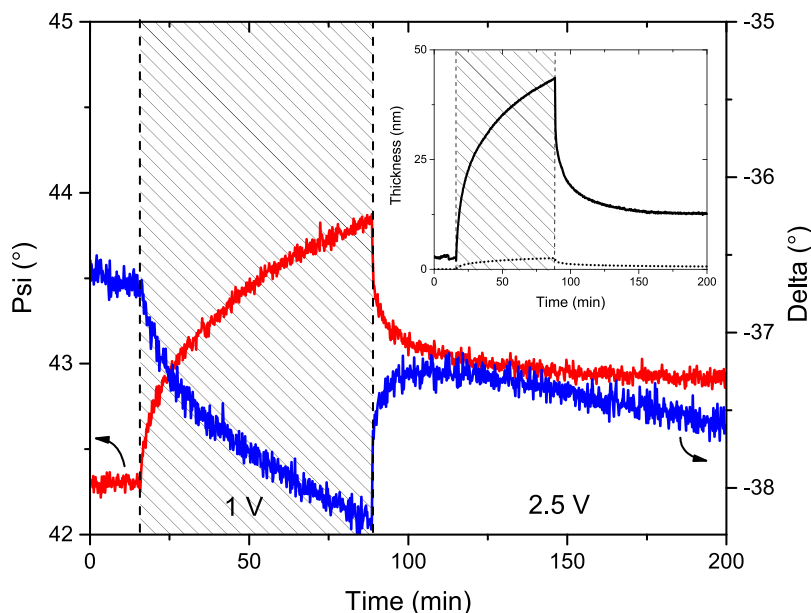


Fig. 5. Time dependence of the ellipsometric angles of a carbon thin film sample in EC:DMC 1:1 + 1 M LiPF₆, during subsequent exposure to 1.0 and 2.5 V versus a Li counter electrode. Psi angles are indicated in red, while Delta angles are shown in blue. Inset: Fitted thickness of SEI (solid line) and Interlayer (dotted line). The fits were performed in the Cauchy region (600–1000 nm) where there was minimal depolarization.

switched back to 2.5 V it partially dissolves. The model seems to overestimate the SEI thicknesses however (with a maximum of around 43 nm), which may be due to the actual refractive indices being higher.

Consistency with the observed changes in the rheological properties implies that the layer must also weaken the attractive forces that hold the KB network together. In the electrostatically screening environment of the 1 M salt solution this is possible through reduced van der Waals attractions. Assuming that the (typical) contact geometry between two sticking KB units remains the same, this would suggest a lowered Hamaker constant.

It may seem surprising that we observe strong effects of a SEI layer within the ‘safe’ operating range of the electrolyte. This may

be due to an uneven current distribution caused by the inhomogeneity of fluid electrodes. This could lead to variations in local particle states of charge, triggering reductive electrolyte decomposition and SEI formation [27–29].

On cycling the fluid electrode to lower voltages, a thicker SEI forms, with a drastic effect on the electronic resistance. It should be noted that the increase in the electronic resistance due to charging (lithiation), is larger than indicated by the LFRI. This is easily recognized from Figs. 3 B and 4 B, in which the low-frequency semi-circle is far from complete at 0.01 Hz, in particular for the lithiated state. The large difference (more than one order of magnitude) in the LFRI between 1.0 V–2.5 V and 0.8 V–2.5 V of the fluid electrode only containing KB indicates that the difference in

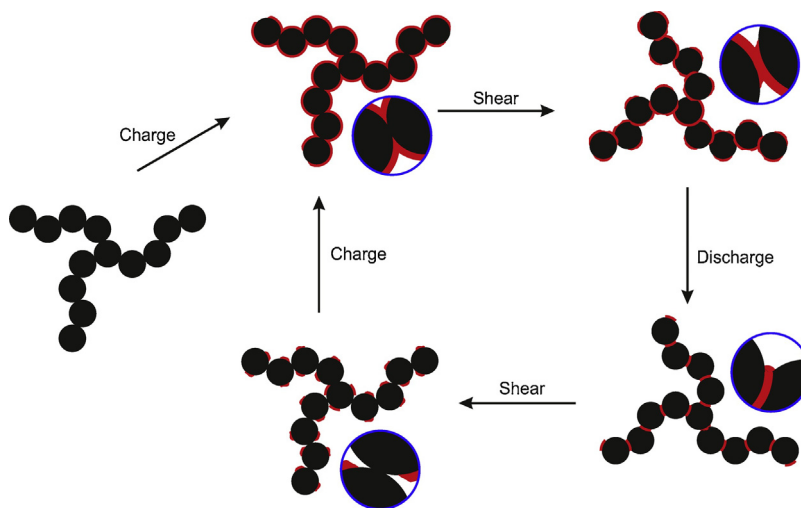


Fig. 6. Proposed mechanism to explain the observed combined effect of (dis)charging to higher potentials and subsequent mechanical rejuvenation on the LFRI (i.e. the conductivity of the KB network). Red color indicates (in an exaggerated way) the presence of an SEI layer, which grows during charging, and shrinks during discharging. Particle contacts are less strongly affected by layer deposition or dissolution. Note: in reality the primary KB particles are fractal-like, and re-assembly after shear leads to a different (but statistically equivalent) network.

electronic conductance must be huge, even for voltages $\geq 1.0\text{ V}$ vs the Li counter electrode. At lower (more reducing) voltages, the effect of the irreversible process on the electronic resistance is probably even larger.

To further examine the formation of surface layers, we compare the LFRI before (open symbols) and after (closed symbols) mechanical rejuvenation in Figs. 3 and 4. For both samples it is clear that restructuring by shear (followed by rest), consistently increases the LFRI after charging and decreases it after discharging. Assuming that the pre-shear breaks down all agglomerates, and that the re-agglomeration process is not impeded by energy barriers (diffusion limited agglomeration [30]), the micro-structure after rejuvenation will (statistically) be the same. However, the conductivity of interparticle contacts will have changed. This is because the contacts between single particles of the network are less likely to be affected by the formation or dissolution of SEI, as they are less exposed to the electrolyte solution. Consequently, less SEI is formed at the contacts during charging (lithiation) and likewise less is dissolved during discharging (delithiation). Mechanical rejuvenation leads to randomization of the contacts. Thus, the subsequently formed contacts will contain mainly

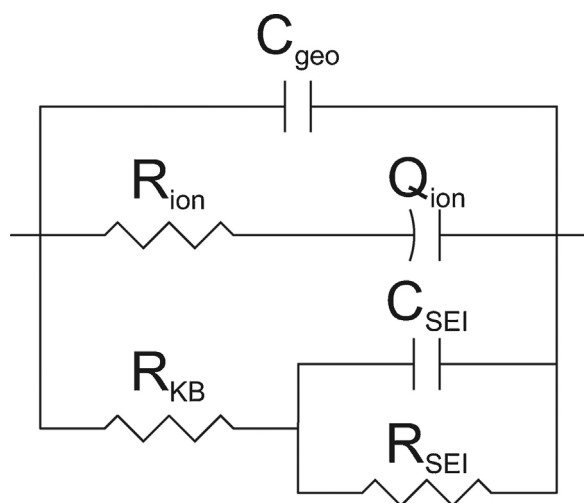


Fig. 7. Equivalent circuit used to fit the data of Fig. 4.

maximally grown (or maximally dissolved) SEI. This mechanistic explanation, illustrated in Fig. 6, thus supports that the formation of the insulating SEI is partially reversible at higher potentials, i.e. lower state of charge. We remark here that the observed reversibility very likely depends on the duration that the fluid electrode potential is held outside of the electrochemical stability window of the electrolyte. Also, as the reversibility of the SEI (and its composition) depends on the potential at which it is formed, this mechanism is no longer valid at very low potentials (0.6 V) where permanent SEI is formed.

The identification of SEI as the cause of impedance changes makes it interesting to extract the electronic resistances by modelling the impedance spectra of the KB only system using a simplified equivalent circuit (Fig. 7). The ionic contribution can be modeled as an ionic resistance R_{ion} in series to a constant phase element Q_{ion} that represents the double layer capacitances of the electrolyte interfaces. To model the electronic part, we use a resistor R_{KB} that represents the summed KB intra-particle resistances in series with a parallel resistor R_{SEI} and capacitor C_{SEI} that accounts for the summed interparticle impedances (due to SEI). A capacitor C_{geo} in parallel to the rest of the circuit represents the geometric capacitance of the system. The fits (Fig. 4B inset) show good agreement with the spectra.

We also note that the measured LFRI and the fitted electronic resistance (the sum of the KB inter and intra particle resistances) in Fig. 8A show the same trends, thereby justifying our earlier given interpretation of the changes in LFRI. Clearly, and as expected, the measured LFRI values under predict the electronic resistance for most lithiated states. In Fig. 8B we decompose the fitted LFRI values into the contributions R_{KB} and R_{SEI} . This comparison shows that the most important changes in the total electronic resistance comes from the interparticle resistance.

4. Conclusions

Our study of the effect of cycling on the rheo-impedance of a LTO-based SSFB anolyte has produced several new insights. Two key properties are very sensitive to the electrochemical state and history: lithiation causes the electronic resistance (LFRI) to increase and the yield stress to decrease, and vice versa for delithiation. A lithiation voltage below 1.0 V vs a Li electrode causes a drastic increase in LFRI. A suspension of only KB particles responds in a similar way to electrochemical state and history, indicating that the observed effects of cycling can be largely

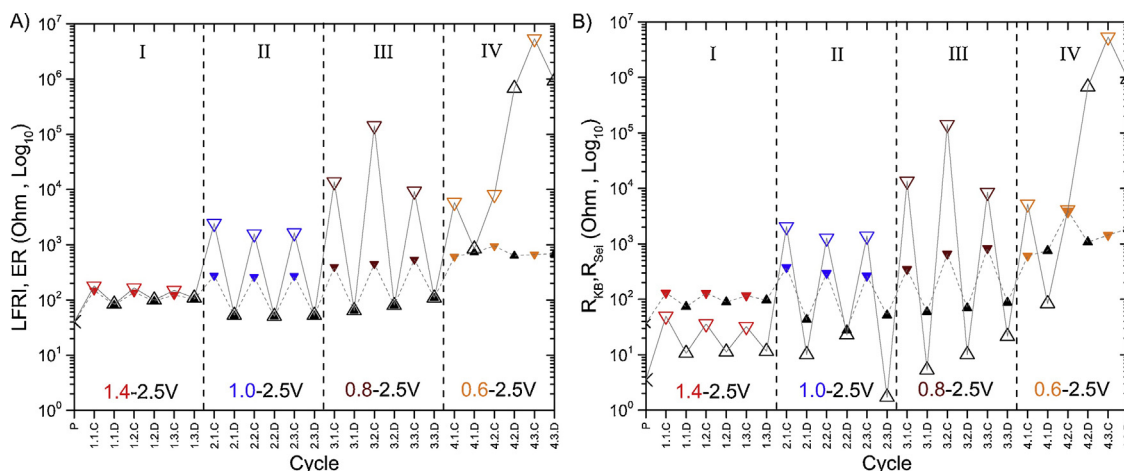


Fig. 8. Results of the fits of spectra of the mechanically rejuvenated samples in Fig. 4A. A) Comparison of total electronic resistance and LFRI. B) Comparison of fit summed KB interparticle (R_{SEI}) and intraparticle (R_{KB}) electronic resistances.

attributed to the KB. A simple mechanistic picture that captures most findings, is one in which the KB particles get covered by a SEI layer during charge (lithiation). For less reducing, i.e. higher voltages, a part of this layer dissolves during discharge. The layer electrically insulates the KB particles and diminishes their attractions. The contact points between the KB units are less affected by the layer growth, similar to conventional solid lithium batteries. However, in SSFBs, a mechanical rejuvenation of the structure takes place every time the fluid gets pumped, leading to the incorporation of the thicker layers into the KB backbone. For strongly reducing voltages a permanent SEI layer is formed.

The implications of our findings for SSFBs are significant. A low electronic resistance is crucial to battery performance, and a sufficient yield stress is required to suspend active materials. Both these properties are adversely affected by SEI formation under the explored experimental conditions. Our findings show that further research into chemistries with absolutely no (insulating) layer formation would be required to realize SSFBs.

Acknowledgements

We acknowledge Prof. Nieck Benes of the Films in Fluids group and Prof. Wiebe de Vos of the Membrane Science and Technology Group at the University of Twente for granting access to the ellipsometer. The research leading to these results has received funding from the European Union Seventh Framework Programme (FP7/2007–2013) under grant agreement n° 608621.

Appendix A. Supplementary data

Supplementary data associated with this article can be found, in the online version, at <http://dx.doi.org/10.1016/j.electacta.2017.08.022>.

References

- [1] M. Duduta, B. Ho, V.C. Wood, P. Limthongkul, V.E. Brunini, W.C. Carter, Y.M. Chiang, *Adv. Energy Mater.* 1 (2011) 511–516.
- [2] K.B. Hatzell, M. Boota, Y. Gogotsi, *Chemical Society Reviews* 44 (2015) 8664–8687.
- [3] A. Narayanan, F. Mugele, M.H.G. Duits, *Langmuir* 33 (7) (2017) 1629–1638, doi: <http://dx.doi.org/10.1021/acs.langmuir.6b04322>.
- [4] M. Youssry, L. Madec, P. Soudan, M. Cerbelaud, D. Guyomard, B. Lestriez, *Phys Chem Chem Phys* 15 (2013) 14476–14486.
- [5] M. Youssry, L. Madec, P. Soudan, M. Cerbelaud, D. Guyomard, B. Lestriez, *Journal of Power Sources* 274 (2015) 424–431.
- [6] Y. Zhang, A. Narayanan, F. Mugele, M.A.C. Stuart, M.H. Duits, *Colloids and surfaces A: Physicochemical and engineering aspects* 489 (2016) 461–468.
- [7] C.R. Fell, L. Sun, P.B. Hallac, B. Metz, B. Sisk, *Journal of The Electrochemical Society* 162 (2015) A1916–A1920.
- [8] J. Vetter, P. Novák, M. Wagner, C. Veit, K.-C. Möller, J. Besenhard, M. Winter, M. Wohlfahrt-Mehrens, C. Vogler, A. Hammouche, *Journal of power sources* 147 (2005) 269–281.
- [9] X. Han, M. Ouyang, L. Lu, J. Li, Y. Zheng, Z. Li, *Journal of Power Sources* 251 (2014) 38–54.
- [10] F.Y. Fan, W.H. Woodford, Z. Li, N. Baram, K.C. Smith, A. Helal, G.H. McKinley, W. C. Carter, Y.-M. Chiang, *Nano letters* 14 (2014) 2210–2218.
- [11] Z. Qi, G.M. Koenig, *Journal of Power Sources* 323 (2016) 97–106.
- [12] T.J. Petek, N.C. Hoyt, R.F. Savinell, J.S. Wainright, *Journal of Power Sources* 294 (2015) 620–626.
- [13] T. Ohzuku, A. Ueda, N. Yamamoto, *Journal of the Electrochemical Society* 142 (1995) 1431–1435.
- [14] E. Ventosa, G. Zampardi, C. Flox, F. La Mantia, W. Schuhmann, J. Morante, *Chemical Communications* 51 (2015) 14973–14976.
- [15] L. Lombardo, S. Brutti, M.A. Navarra, S. Panero, P. Reale, *Journal of Power Sources* 227 (2013) 8–14.
- [16] Y.R. Dougassa, J. Jacquemin, L. El Ouatani, C.c. Tessier, M.r.m. Anouti, *The Journal of Physical Chemistry B* 118 (2014) 3973–3980.
- [17] E. Barsoukov, J.R. Macdonald, *Impedance spectroscopy: theory, experiment, and applications*, John Wiley & Sons, 2005.
- [18] L. Callegaro, *Electrical impedance: principles, measurement, and applications*, CRC Press, 2012.
- [19] B. Burrows, R. Jasinski, *Journal of the Electrochemical Society* 115 (1968) 365–367.
- [20] F. La Mantia, C. Wessells, H. Deshazer, Y. Cui, *Electrochemistry Communications* 31 (2013) 141–144.
- [21] G. Schramm, *A practical approach to rheology and rheometry*, Haake Karlsruhe, 1994.
- [22] J. Jamnik, J. Maier, *Journal of The Electrochemical Society* 146 (1999) 4183–4188.
- [23] P. Lu, C. Li, E.W. Schneider, S.J. Harris, *The Journal of Physical Chemistry C* 118 (2014) 896–903.
- [24] S.J. An, J. Li, C. Daniel, D. Mohanty, S. Nagpure, D.L. Wood, *Carbon* 105 (2016) 52–76.
- [25] J. Collins, G. Gourdin, M. Foster, D. Qu, *Carbon* 92 (2015) 193–244.
- [26] M. McArthur, S. Trussler, J. Dahn, *Journal of the Electrochemical Society* 159 (2012) A198–A207.
- [27] T. Nishi, H. Nakai, A. Kita, *Journal of The Electrochemical Society* 160 (2013) A1785–A1788.
- [28] J. Nanda, J. Remillard, A. O'Neill, D. Bernardi, T. Ro, K.E. Nietering, J.Y. Go, T.J. Miller, *Advanced Functional Materials* 21 (2011) 3282–3290.
- [29] W.C. Chueh, F. El Gabaly, J.D. Sugar, N.C. Bartelt, A.H. McDaniel, K.R. Fenton, K.R. Zavadil, T. Tylliszczak, W. Lai, K.F. McCarty, *Nano letters* 13 (2013) 866–872.
- [30] M. Cerbelaud, B. Lestriez, R. Ferrando, A. Videcoq, M. Richard-Plouet, M.T. Caldes, D. Guyomard, *Langmuir* 30 (2014) 2660–2669.